Supporting Information

Isomeric thermally activated delayed fluorescence emitters for highly efficient organic light-emitting diodes

Yanyan Liu,[†a] Jiaji Yang,[†b] Zhu Mao,*[c] Yuyuan Wang,[a] Juan Zhao,*[d] Shi-Jian Su*[b],and Zhenguo Chi*[a]

Y. Liu, D. Ma, Y. Wang, Prof. Z. Chi
PCFM Lab, GDHPPC Lab, Guangdong Engineering Technology Research Center for High-performance Organic and Polymer Photoelectric Functional Films, State Key Laboratory of OEMT, School of Chemistry, Sun Yat-sen University
Guangzhou 510275, China
E-mail: chizhg@mail.sysu.edu.cn

J. Yang, Prof. S.-J. Su.
State Key Laboratory of Luminescent Materials and Devices and Institute of Polymer Optoelectronic Materials and Devices, South China University of Technology, Guangzhou 510640, China
E-mail: mssjsu@scut.edu.cn

Prof. Z. Mao
Shenzhen Institute of Advanced Electronic Materials, Shenzhen Institutes of Advanced Technology, Chinese Academy of Sciences, Shenzhen 518055, China
E-mail: maozhu1989@hotmail.com
Prof. J. Zhao
School of Materials Science and Engineering, Sun Yat-sen University, Guangzhou 510275, China
E-mail: zhaoj95@mail.sysu.edu.cn

Table of Contents

I. Experimental Procedures

General Methods

Hydrogen (^{1}H) and carbon (^{13}C) nuclear magnetic resonance (NMR) spectra were measured using a Bruker AvanceIII 400HD and 600HD spectrometer, with deuterated chloroform ($CDCl_3$) and dimethylsulfoxide (DMSO-d_6) as solvent and tetramethylsilane (TMS) as an internal reference. High resolution mass spectra (HRMS) were collected from Thermo Orbitrap Tribrid spectrometer. Photoluminescence (PL) spectra and UV-vis absorption spectra were measured using a Shimadzu RF-5301PC spectrometer and a Hitachi U-3900 spectrophotometer, respectively. Transient PL decay characteristics were recorded on measured by Edinburgh FLS 980 spectrometer. The PL quantum yields were measured on a Hamamatsu C9920-02G absolute PL quantum yield measurement system. Differential scanning calorimetry was performed using a NETZSCH DSC 214 Polyma DSC2140A-0211-L at a heating rate of 20 ˚C min^{-1} under N_2 atmosphere. Thermogravimetric analyses were conducted with a TA thermal analyzer (A50) under N_2 atmosphere with a heating rate of 20 ˚C min^{-1}. Cyclic voltammetry measurements were carried out on an electrochemical workstation VMP300 (Bio-Logic), by using tetrabutylammoniumhexafluorophosphate ($TBAPF_6$, 0.1 M) in dichloromethane as electrolyte, a platinum as counter electrode, and a Ag/AgCl as reference electrode (versus ferrocene F_c/F_c^+). Time-dependent density functional theory (TD-DFT) calculations were performed with Gaussian 09W program package and produced by B3LYP/6-311G(*).[1] Spin-orbital coupling matrix elements were investigated by PySOC program based on the TD-DFT results.[2] NTO and electron density analysis were extracted by the Multiwfn (version 3.8) and plotted via VMD software (version 1.9.3) based on the TD-DFT results.[3, 4]

Devices Fabrication and Characterization.

Indium tin oxide (ITO) coated glass substrates were firstly ultrasonically cleaned with detergent, deionized water, acetone and isopropyl alcohol in sequence, and treated with O_2 plasma for 15 min after drying. Then, the ITO substrates were transferred to a thermal evaporation chamber for deposition of organic and metals layers under high vacuum (~10^{-5} Pa). Organic materials were deposited successively on ITO glass substrate with evaporation rate of 1-2 Å s^{-1}. The LiF and aluminum were deposited with an evaporation rate of 0.05-0.1 Å s^{-1} and 1-5 Å s^{-1}, respectively. The light emission area of devices is 3 mm×3 mm. Current density-voltage-luminance characteristics, electroluminescence (EL) spectra and device efficiencies were simultaneously measured with a computer-controlled Keithley 2450 power source and a PR-745 spectral radiometer.

TADF Parameters calculation.

The key rate constants of TADF process were calculated based on the following equations (1) − (6):[5]

TADF parameters equations:

$$K_{r(PF)} = \frac{\Phi_{PF}}{\tau_{PF}} \quad (1)$$

$$k_{DF} = \frac{\Phi_{DF}}{\tau_{DF}} \quad (2)$$

$$k_{ISC} = \frac{\Phi_{DF}}{\Phi_{PF} + \Phi_{DF}}.k_{PF} \quad (3)$$

$$k_{RISC} = \frac{k_{DF}k_{PF}}{K_{ISC}}.\frac{\Phi_{DF}}{\Phi_{PF}} = \frac{k_{DF}\Phi_{RISC}}{1 - \Phi_{ISC}\Phi_{RISC}} \quad (4)$$

$$\Phi_{ISC} = \frac{K_{ISC}}{K_{PF}} \quad (5)$$

$$k_{nr} = \frac{K_{RISC}}{\Phi_{RISC}} - k_{RISC} \quad (6)$$

where Φ_{PF}, τ_{PF} and Φ_{DF}, τ_{DF} are the quantum efficiency and fluorescence lifetime of prompted (PF) and delayed emissions (DF), respectively. $K_{r(PF)}$ and k_{DF} are the rate constant of prompted and delayed fluorescence. k_{ISC} and k_{RISC} are the rate constant of intersystem crossing and reverse intersystem crossing. k_{nr} is the rate constant of nonradiative decay for singlet excited state.

Synthesis and characterization

The compounds of NTPZ and TNPZ were synthesized following Scheme S1 as below:

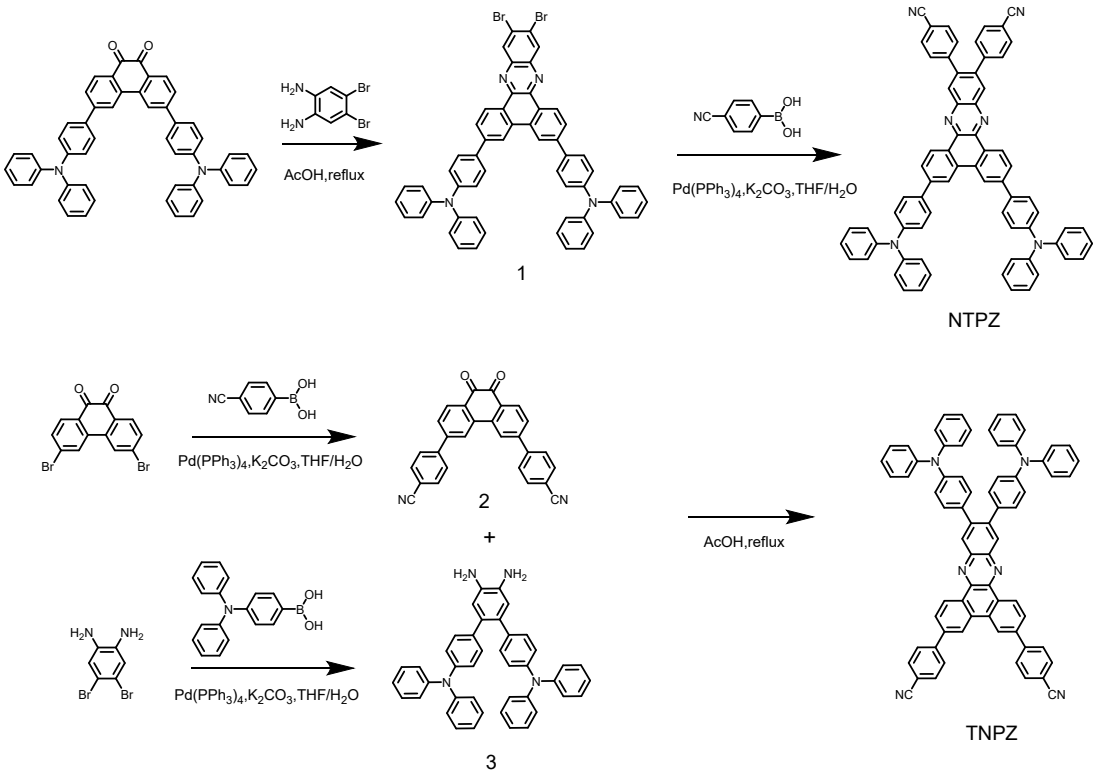

Scheme S1. Synthetic routes of NTPZ and TNPZ

Synthesis of 4,4'-(11,12-dibromo-11,12-dihydrodibenzo[a,c]phenazine-3,6-diyl)bis-(N,Ndiphenylaniline) (1)

3,6-bis(4-(diphenylamino)phenyl)phenanthrene-9,10-dione (694 mg, 1 mmol) and 4,5-dibromobenzene-1,2-diamine (293 mg, 1.1 mmol) dissolved in AcOH (20 mL), then the mixture was refluxed overnight. After cooling to room temperature, the resulting mixture was poured into ice-water (200 mL), and then filtered, the crude product is

recrystallized in ethanol. Yield 86%. ^{1}H NMR was not obtained due to low solubility. HRMS(EI) m/z: [M] $^+$ calcd for $C_{56}H_{38}Br_2N_4$, 924.1286, found 924.1294.

Synthesis of 4,4'-(3,6-bis(4-(diphenylamino)phenyl)dibenzo[a,c]phenazine-11,12-diyl)dibenzonitrile (NTPZ)

Compound 1 (922 mg, 1 mmol) and 4-Cyanophenylboronic acid (324 mg, 2.2 mmol) were dissolved in THF (25 mL), then 2 M K_2CO_3 solution (5mL) was added. Then catalytic amount of $Pd(PPh_3)_4$ was added into the mixture under an argon atmosphere. The resulting mixture was stirred at 80 ˚C for 24 h. After cooling down to ambient temperature, the solvents were evaporated under vacuum and the resulting residue was extracted with DCM and water followed by purification by column chromatography with dichloromethane/n-hexane. Yield 63%. ^{1}H NMR (400 MHz, Chloroform-*d*) δ 9.40 (d, *J* = 8.4 Hz, 2H), 8.75 (s, 2H), 8.43 (s, 2H), 7.96 (d, *J* = 8.3 Hz, 2H), 7.67 (dd, *J* = 26.4, 8.2 Hz, 8H), 7.40 (d, *J* = 7.9 Hz, 4H), 7.32 (t, *J* = 7.7 Hz, 8H), 7.24 (d, *J* = 8.4 Hz, 4H), 7.19 (d, *J* = 8.0 Hz, 8H), 7.09 (t, *J* = 7.3 Hz, 4H). ^{13}C NMR (101 MHz, Chloroform-*d*) δ 148.18, 147.44, 144.47, 143.57, 143.32, 141.22, 140.31, 133.85, 132.72, 132.21, 131.11, 130.63, 129.43, 128.30, 128.21, 127.21, 126.86, 124.80, 123.45, 123.41, 120.82, 118.47, 111.61. HRMS (ESI) m/z: $[M+H]^+$ calcd for $C_{70}H_{44}N_6$, 968.3627, found 969.3698. Anal. Calcd for: C, 86.75; H, 4.58; N, 8.67. Found C, 86.10; H, 4.51; N, 8.44.

Synthesis of 4,4'-(9,10-dioxo-9,10-dihydrophenanthrene-3,6-diyl)dibenzonitrile (2):

3,6-Dibromo-9,10-phenanthrenequinone (1.09 g, 3 mmol) and 4-Cyanophenylboronic acid (529 mg, 3.6 mmol) were dissolved in THF (30 mL), then 2 M K_2CO_3 solution (3 mL) was added. Then catalytic amount of $Pd(PPh_3)_4$ was added into the mixture under an argon atmosphere. The resulting mixture was stirred at 80 ˚C for 24 h. After cooling down to ambient temperature, the solvents were evaporated under vacuum and the resulting residue was extracted with DCM and water, followed by purification by column chromatography with dichloromethane/n-hexane. Yield 60%. ^{1}H NMR (400 MHz, DMSO-d_6) δ 8.80 (d, J = 1.9 Hz, 2H), 8.16 (dd, J = 8.4, 1.8 Hz, 6H), 8.09 – 7.99 (m, 4H), 7.93 (dd, J = 8.2, 1.6 Hz, 2H).

Synthesis of N4,N4,N4'',N4''-tetraphenyl-[1,1':2',1''-terphenyl]-4,4',4'',5'-tetraamine (3):

4,5-Dibromobenzene-1,2-diamine (1.33 g, 5 mmol) and 4-(Diphenylamino) Phenylboronic acid (2.17g, 7.5 mmol) were dissolved in THF (50 mL), then 2 M K_2CO_3

solution (5 mL) was added. Then catalytic amount of $Pd(PPh_3)_4$ was added into the mixture under an argon atmosphere. The resulting mixture was stirred at 80 ˚C for 24 h. After cooling down to ambient temperature, the solvents were evaporated under vacuum and the resulting residue was extracted with DCM and water, followed by purification by column chromatography with dichloromethane/n-hexane. Yield 42%. ^{1}H NMR (400 MHz, Chloroform-*d*) δ 7.21 (t, *J* = 7.7 Hz, 8H), 7.06 (d, *J* = 8.0 Hz, 8H), 7.02 – 6.95 (m, 8H), 6.92 (d, *J* = 8.3 Hz, 4H), 6.80 (s, 2H).

Synthesis of 4,4'-(11,12-bis(4-(diphenylamino)phenyl)dibenzo[a,c]phenazine-3,6-diyl)dibenzonitrile (TNPZ)

Compound 1 (410 mg, 1 mmol) and compound 2 (713 mg, 1.2 mmol) dissolved in AcOH (15 mL), then the mixture was refluxed overnight. After cooling to room temperature, the resulting mixture was poured into ice-water (200 mL), and then filtered, the crude product purification was performed by column chromatography with dichloromethane/n-hexane as eluent. Yield 70%.^{1}H NMR (400 MHz, Chloroform-*d*) δ 9.54 (d, J = 8.1 Hz, 2H), 8.76 (s, 2H), 8.41 (s, 2H), 7.99 (d, J = 7.2 Hz, 2H), 7.96 – 7.75 (m, 8H), 7.34 – 7.26 (m, 8H), 7.22 (d, J = 8.2 Hz, 4H), 7.19 – 7.11 (m, 8H), 7.06 (td, J = 8.4, 2.1 Hz, 8H). ^{13}C NMR (151 MHz, Chloroform-*d*) δ 147.55, 147.23, 145.29, 143.93, 141.98, 141.85, 140.98, 134.14, 132.86, 132.00, 130.84, 129.72, 129.38, 128.25, 127.38, 127.27, 124.68, 123.20, 122.62, 121.70, 118.78, 111.71.HRMS m/z: $[M+1]^+$ calcd for $C_{70}H_{44}N_6$, 968.3627, found 969.3702. Anal. Calcd for: C, 86.75; H, 4.58; N, 8.67. Found C, 86.51; H, 4.92; N, 8.41.

II. Results and Discussion

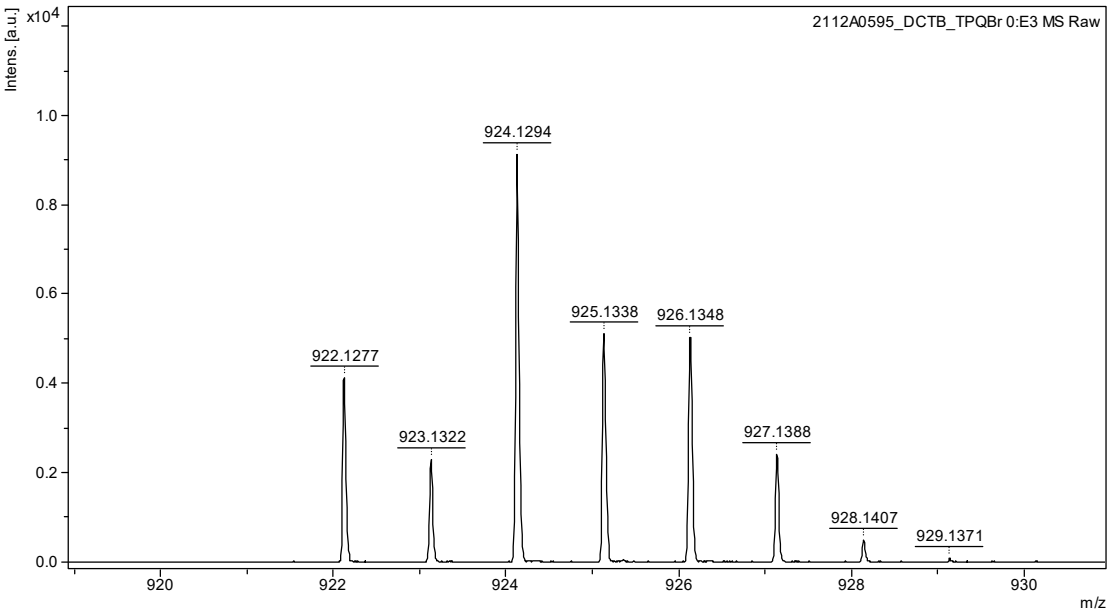

Figure S1. HRMS spectrum of compound 1.

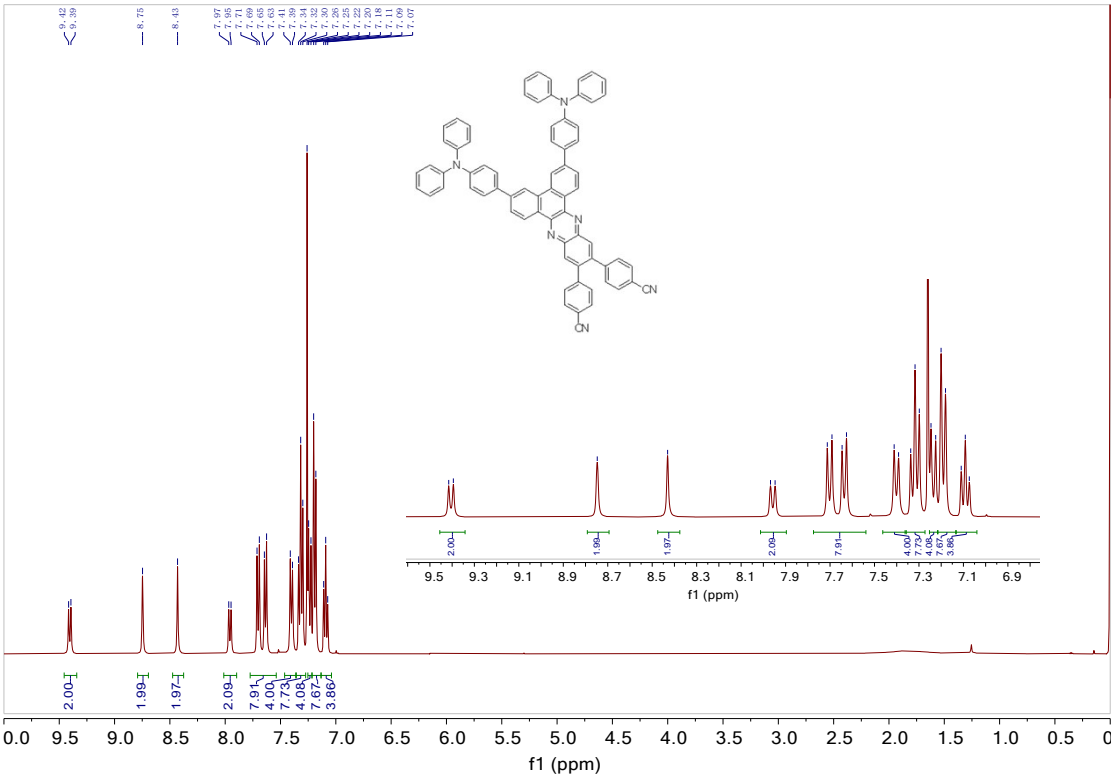

Figure S2. ^{1}H NMR spectrum of NTPZ.

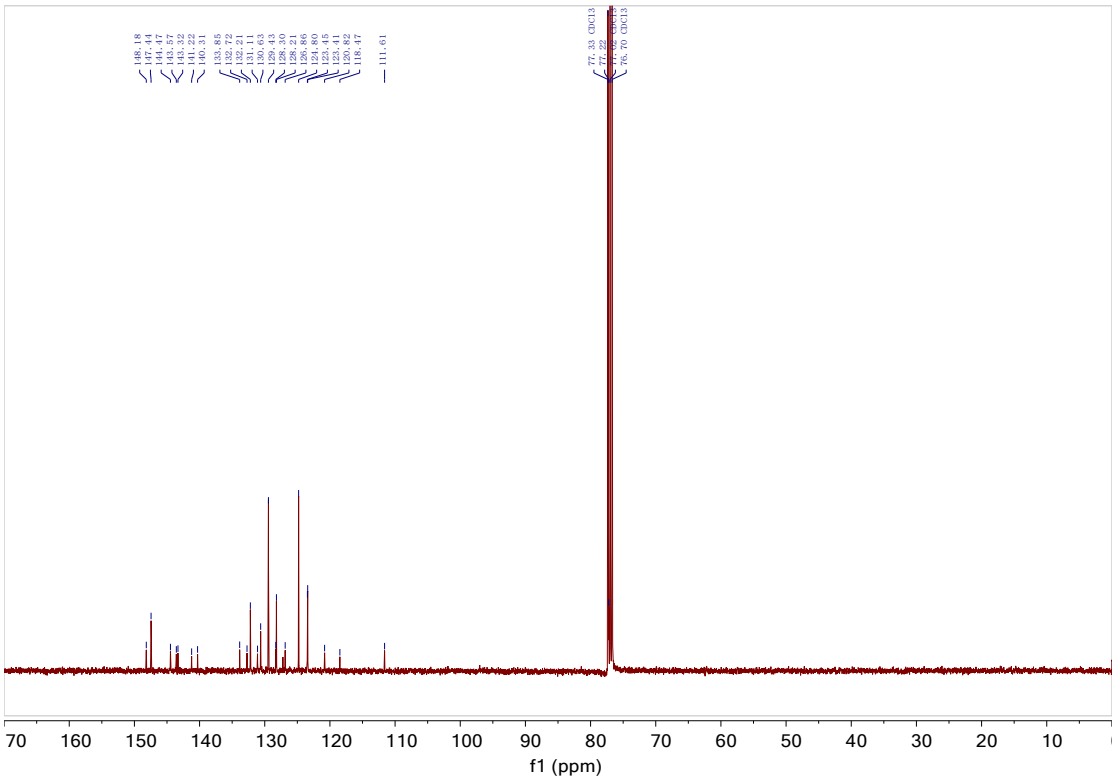

Figure S3. ^{13}C NMR spectrum of NTPZ.

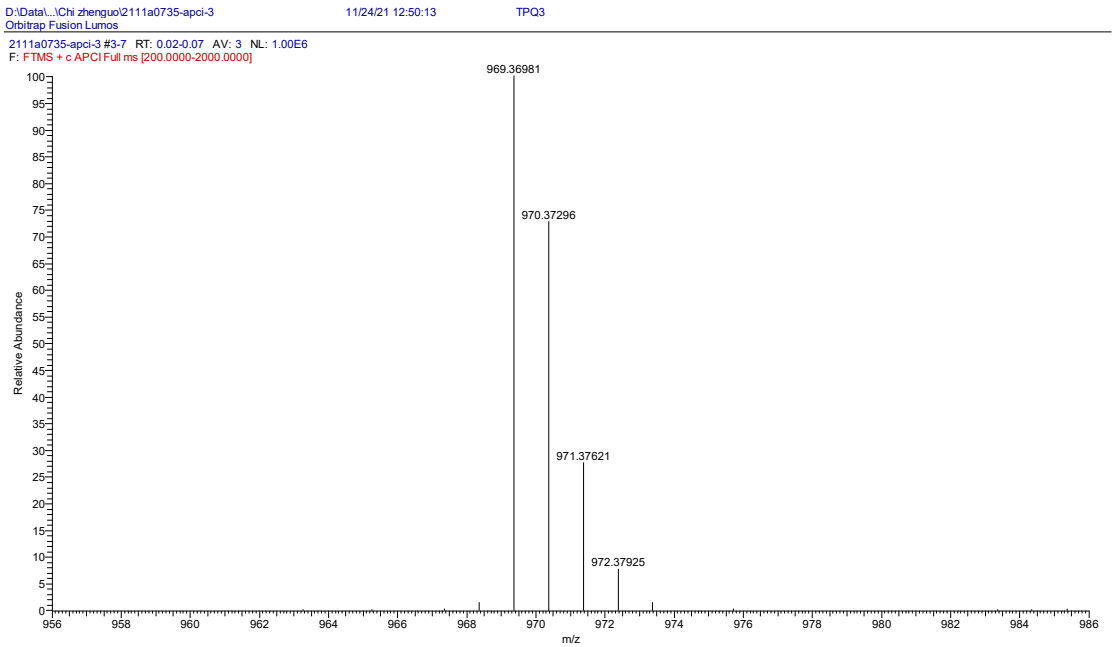

Figure S4. HRMS spectrum of NTPZ.

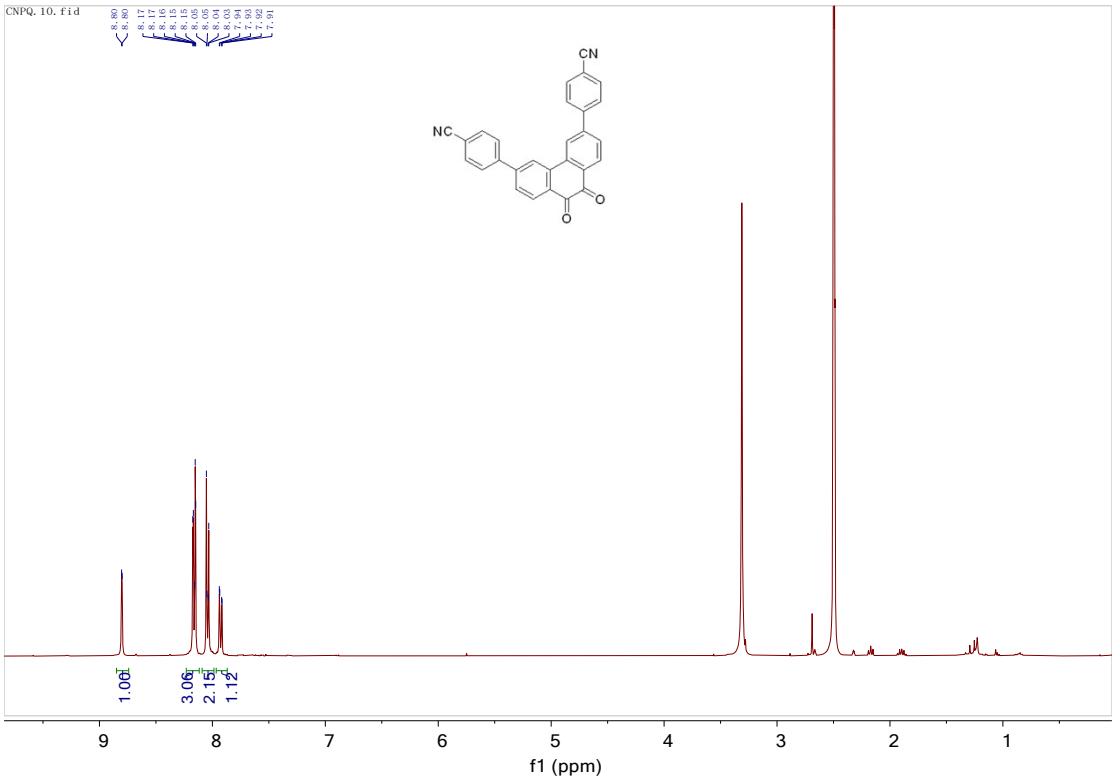

Figure S5. ^{1}H NMR spectrum of compound 2.

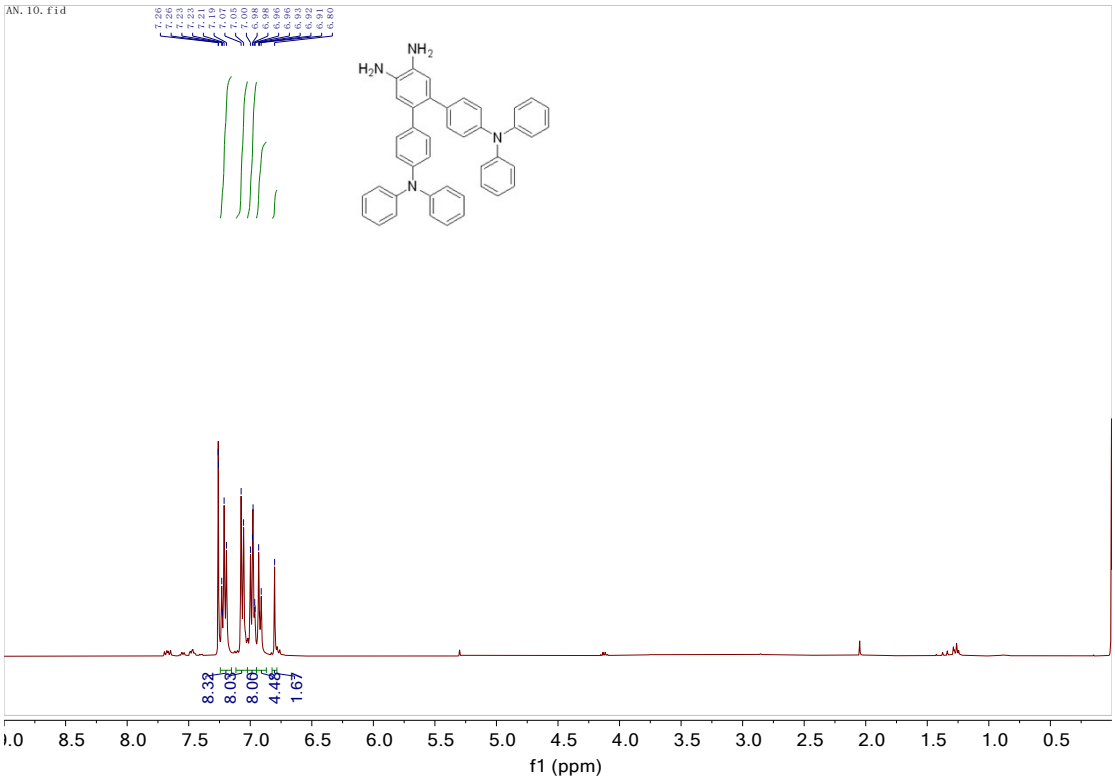

Figure S6. ^{1}H NMR spectrum of compound 3.

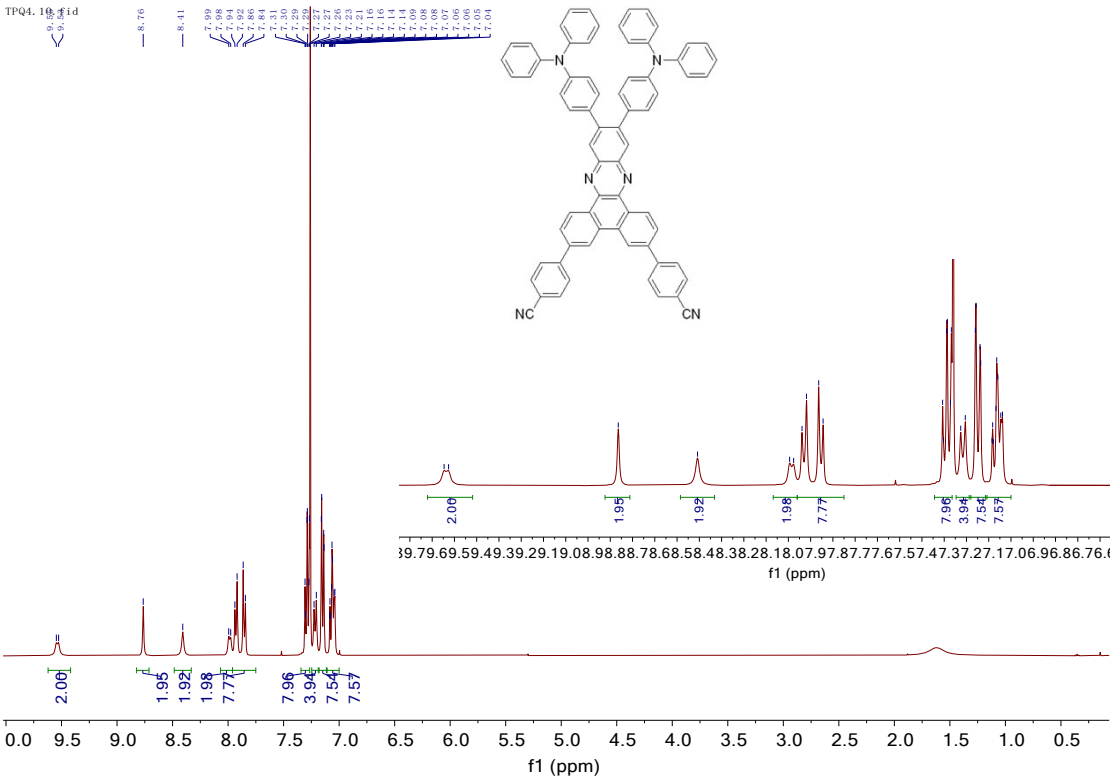

Figure S7. ^{1}H NMR spectrum of TNPZ.

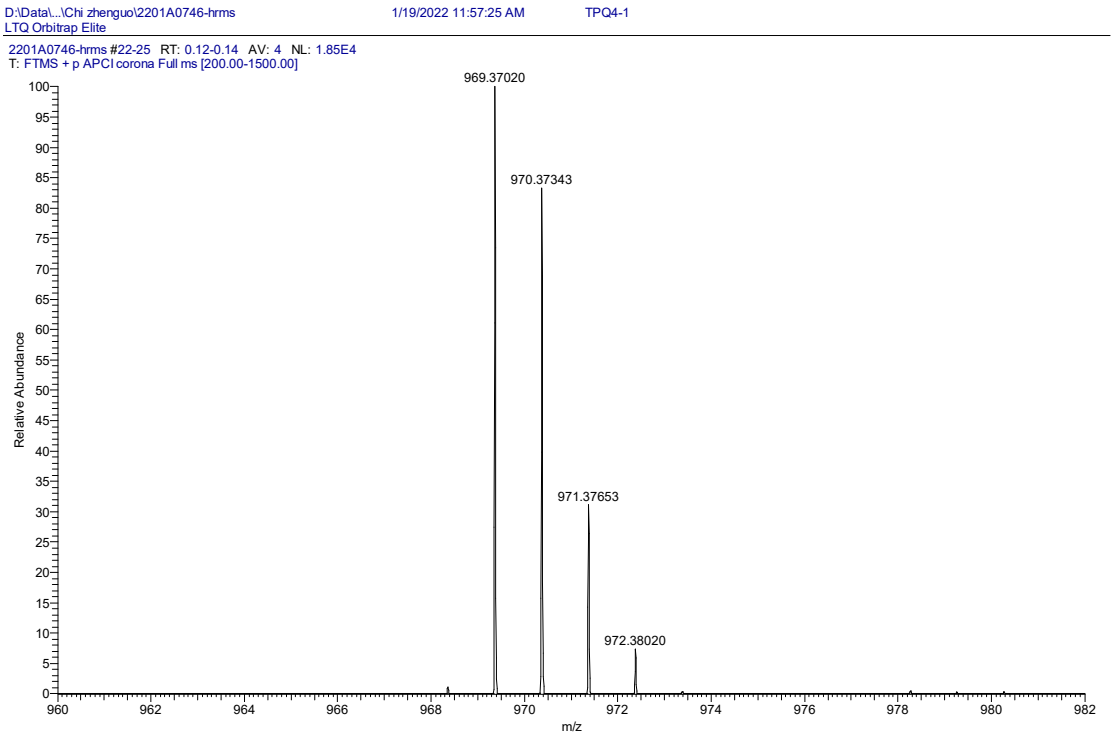

Figure S8. HRMS spectrum of compound TNPZ.

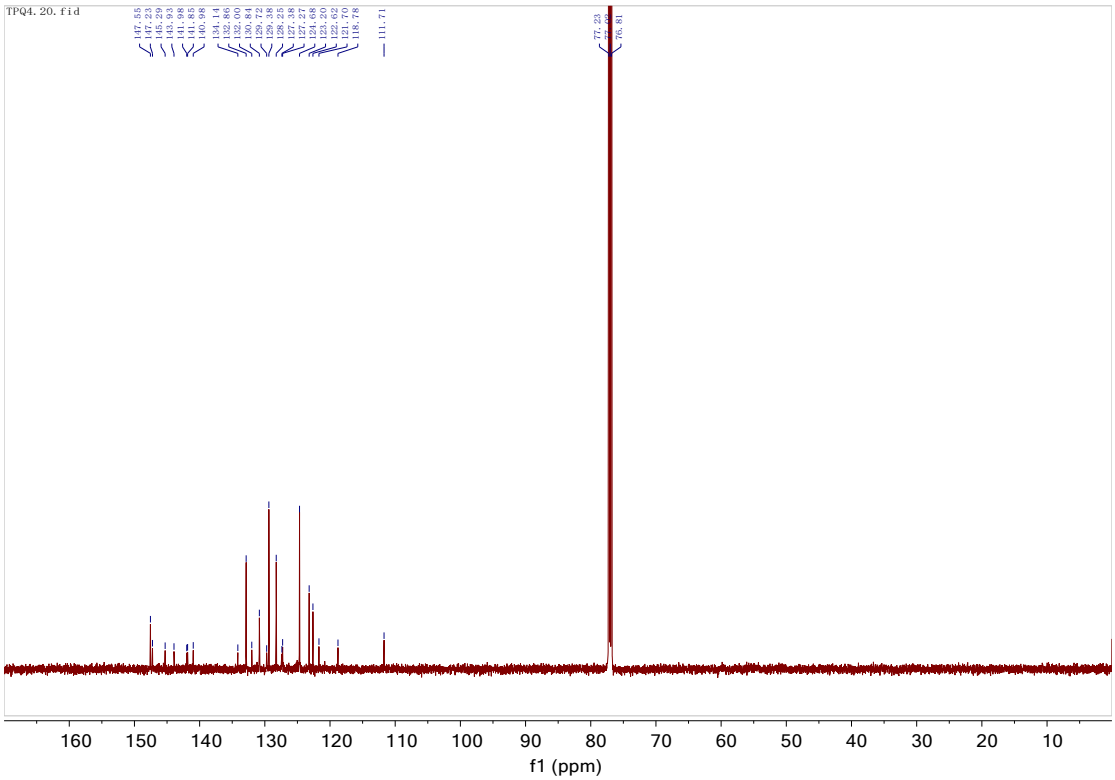

Figure S9. ^{13}C NMR spectrum of TNPZ.

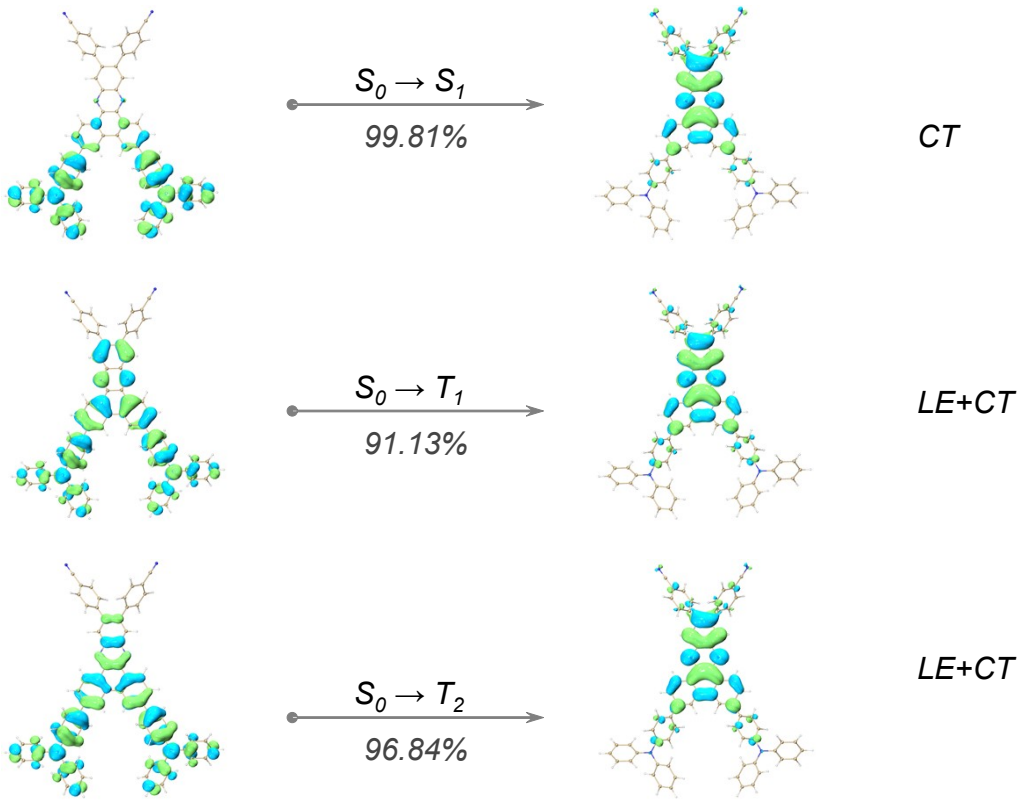

Figure S10. Natural transition orbitals of NTPZ.

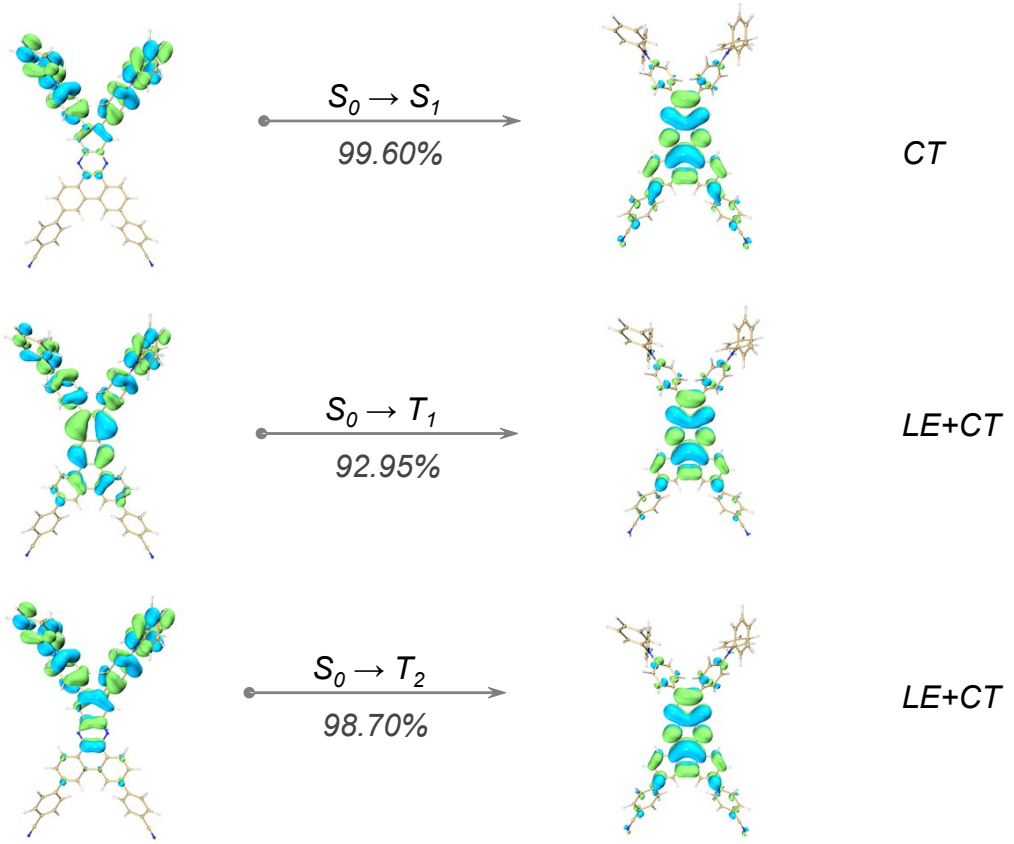

Figure S11. Natural transition orbitals of TNPZ.

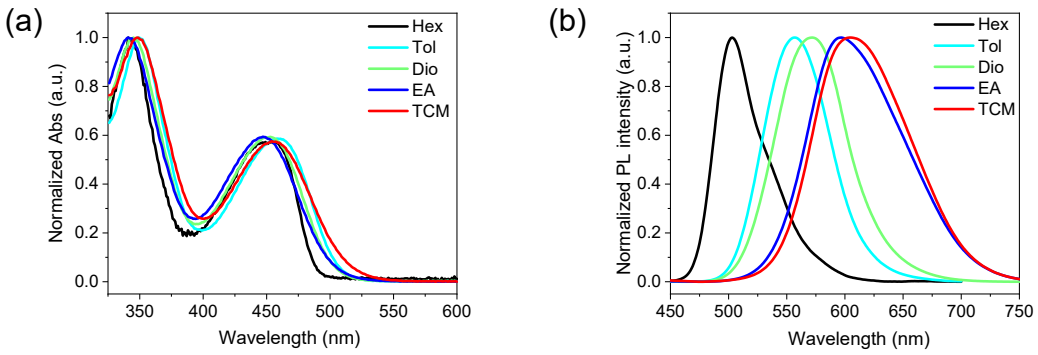

Figure S12. UV-vis absorption (a) and PL (b) spectra of NTPZ.

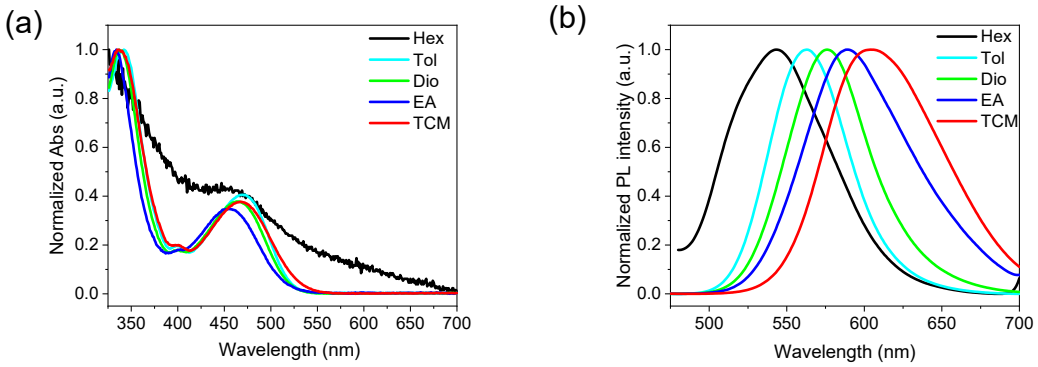

Figure S13. UV-vis absorption (a) and PL (b) spectra of TNPZ.

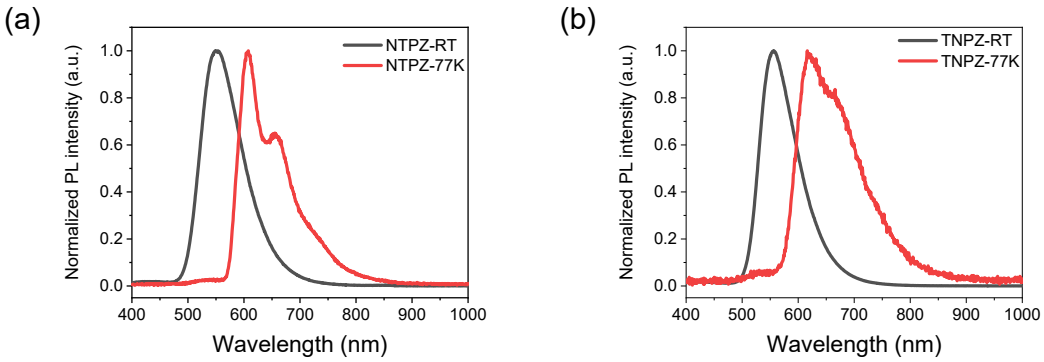

Figure S14. Fluorescence spectra at room temperature and phosphorescence spectra at 77 K for (a) NTPZ and (b) TNPZ in toluene solutions.

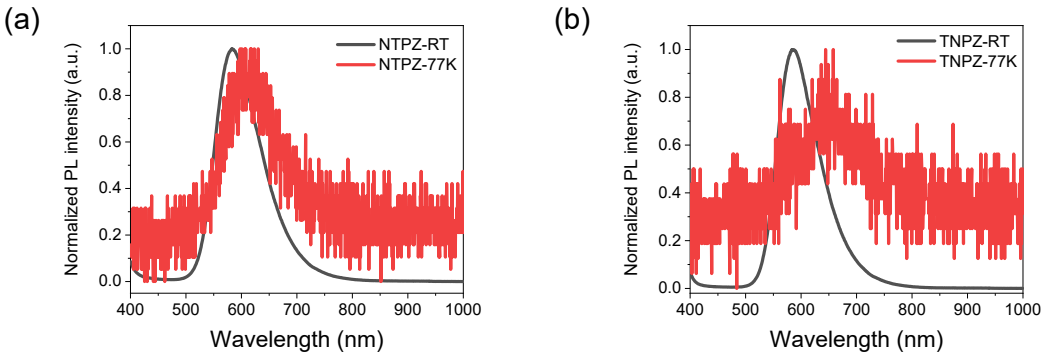

Figure S15. Fluorescence spectra at room temperature and phosphorescence spectra at 77 K for (a) NTPZ and (b) TNPZ in 10 wt% doped CBP films.

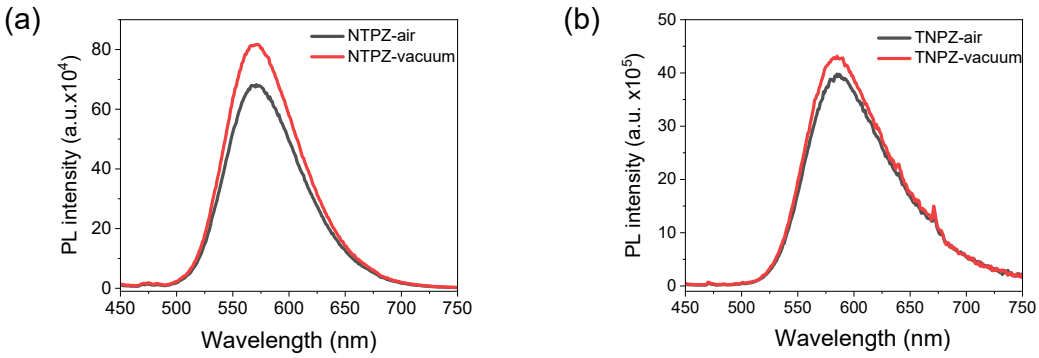

Figure S16. PL spectra in air and vacuum condition for (a) NTPZ and (b) TNPZ in 10 wt% doped CBP films.

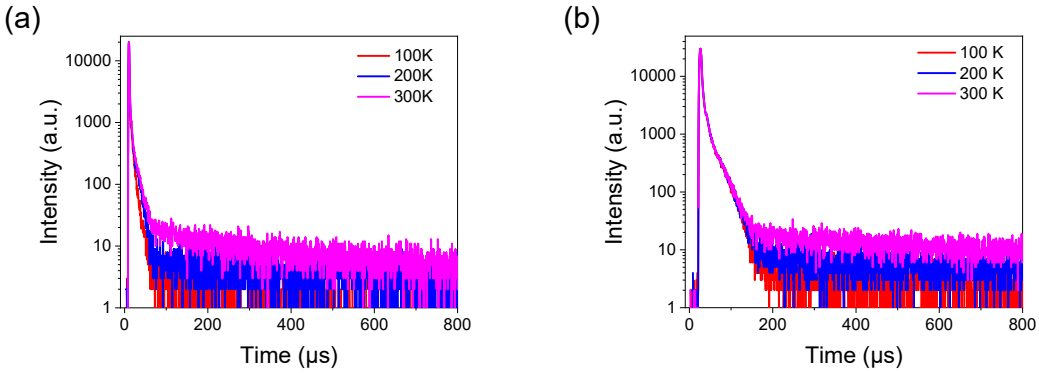

Figure S17. Temperature-dependent transient decays spectra of (a) NTPZ and (b) TNPZ in 10 wt% doped CBP films.

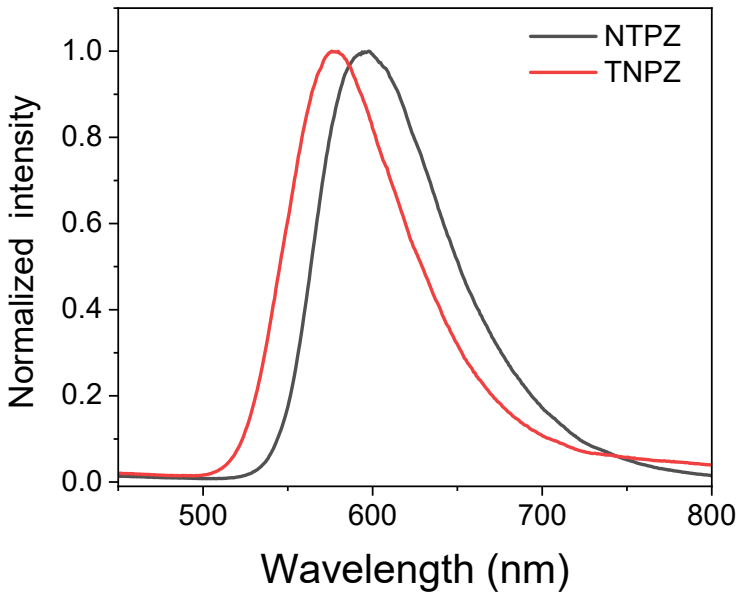

Figure S18. PL spectra of NTPZ and TNPZ in solid powder.

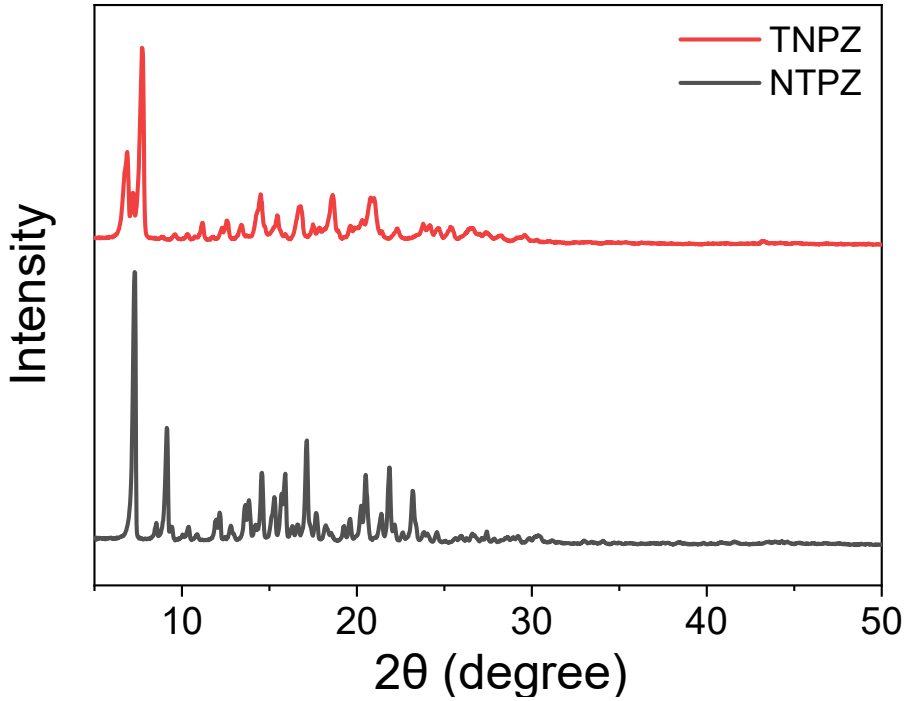

Figure S19. Powder X-ray diffraction of NTPZ and TNPZ.

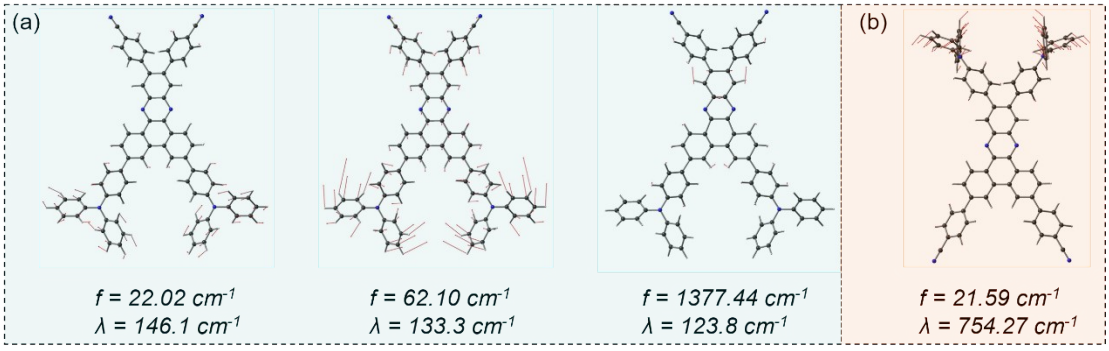

Figure S20. The corresponding main vibration modes of (a) NTPZ and (b) TNPZ.

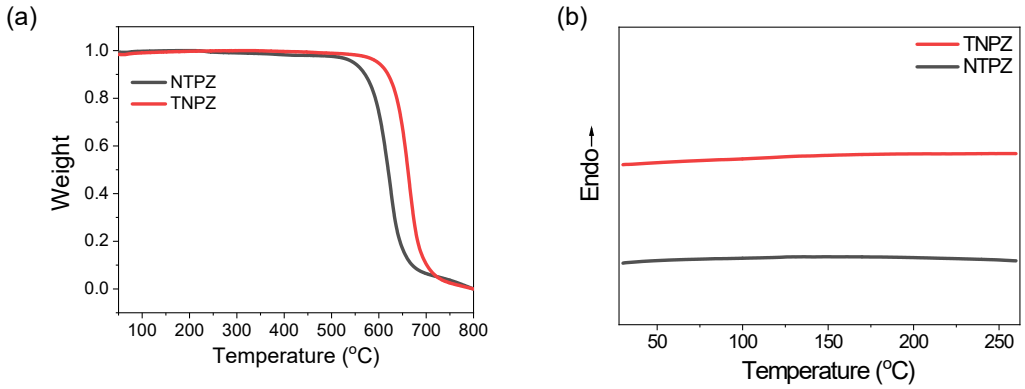

Figure S21. (a) Thermogravimetric analysis curves and (b) differential scanning calorimetry curves of NTPZ and TNPZ.

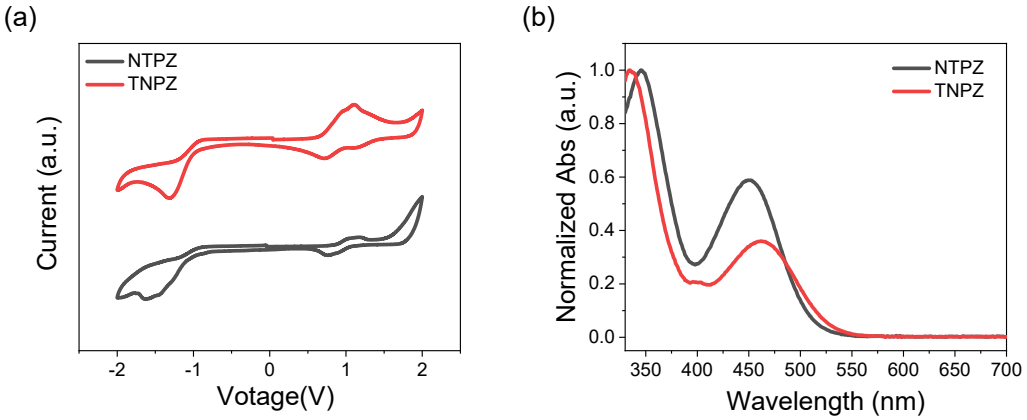

Figure S22. (a) Cyclic voltammetry curves of NTPZ and TNPZ. HOMO is determined by HOMO =−4.8 − (E_{ox}−$E_{1/2(Ferrocene)}$), wherein E_{ox} is the oxidation potential point, $E_{1/2(Ferrocene)}$ is the oxidation potential of ferrocene (F_c/F_{c+}). (b) UV-vis absorption spectra in DCM solutions (1×10^{-5} mol/L) of the molecules.

The electrochemical properties of NTPZ and TNPZ were estimated by cyclic voltammetry measurement. As shown in Figure. S22, the HOMO level of NTPZ and TNPZ is estimated to be -5.18 and -5.01 eV, considering their E_g of 2.21 and 2.19 eV, and then the LUMO level is calculated to be -2.21 and -2.19 eV, respectively.

Table S1. EL performances of TADF-OLEDs

EML	V_{on} (V)	L_{max} (cd m^{-2})	CE_{max} (cd A^{-1})	PE_{max} (lm W^{-1})	EQE_{max}/ EQE_{100}/ EQE_{1000} (%)	λ_{EL} (nm)	CIE (x, y)
10 wt% NTPZ:CBP	2.8	6172	82.3	92.3	27.5/5.73/3.04	562	(0.46, 0.53)
10 wt% TNPZ:CBP	3.2	4290	50.0	49.1	18.3/7.07/3.15	582	(0.53, 0.47)

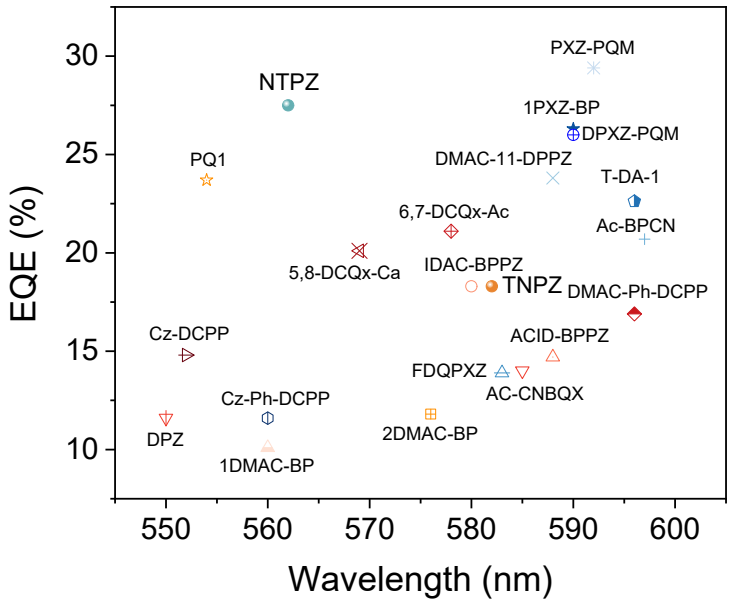

Figure S23. EQE summary of TADF materials based on the similar backbone with EL spectral peaks of 550-600 nm.

Table S2. Device performance summary of emitters listed in Figure S23.

Name	Host	Doping ration (%)	EQE_{max}	EL (nm)	Ref.
1PXZ-BP	CBP	7	26.3	590	6
2DMAC-BP	mCBP	20	11.8	576	7
1DMAC-BP	mCBP	20	10.1	560	7
DMAC-11-DPPZ	CBP	10	23.8	588	8
Ac-BPCN	PBICT	1	20.7	597	9
PQ1	mCBP	2	23.7	554	10
5,8-DCQx-Ca	mCP-PFP	1	20.1	569	11
6,7-DCQx-Ac	mCP-PFP	1	21.1	578	11
T-DA-1	mCBP	10	22.62	596	12
IDAC-BPPZ	CBP	11	18.3	580	13
ACID-BPPZ	CBP	11	14.7	588	13
DPZ	CBP	10	11.6	550	14
FDQPXZ	BePP2	5	13.9	583	15
PXZ-PQM	DCzDPy	5	29.4	592	16
DPXZ-PQM	DCzDPy	5	26.0	590	16
Ac-CNBQX	CBP	6	14.0	585	17
Cz-DCPP	mCPPy2PO	10	14.8	552	18
DMAC-Ph-DCPP	mCPPy2PO	10	16.9	596	18
Cz-Ph-DCPP	mCPPy2PO	10	11.6	560	18

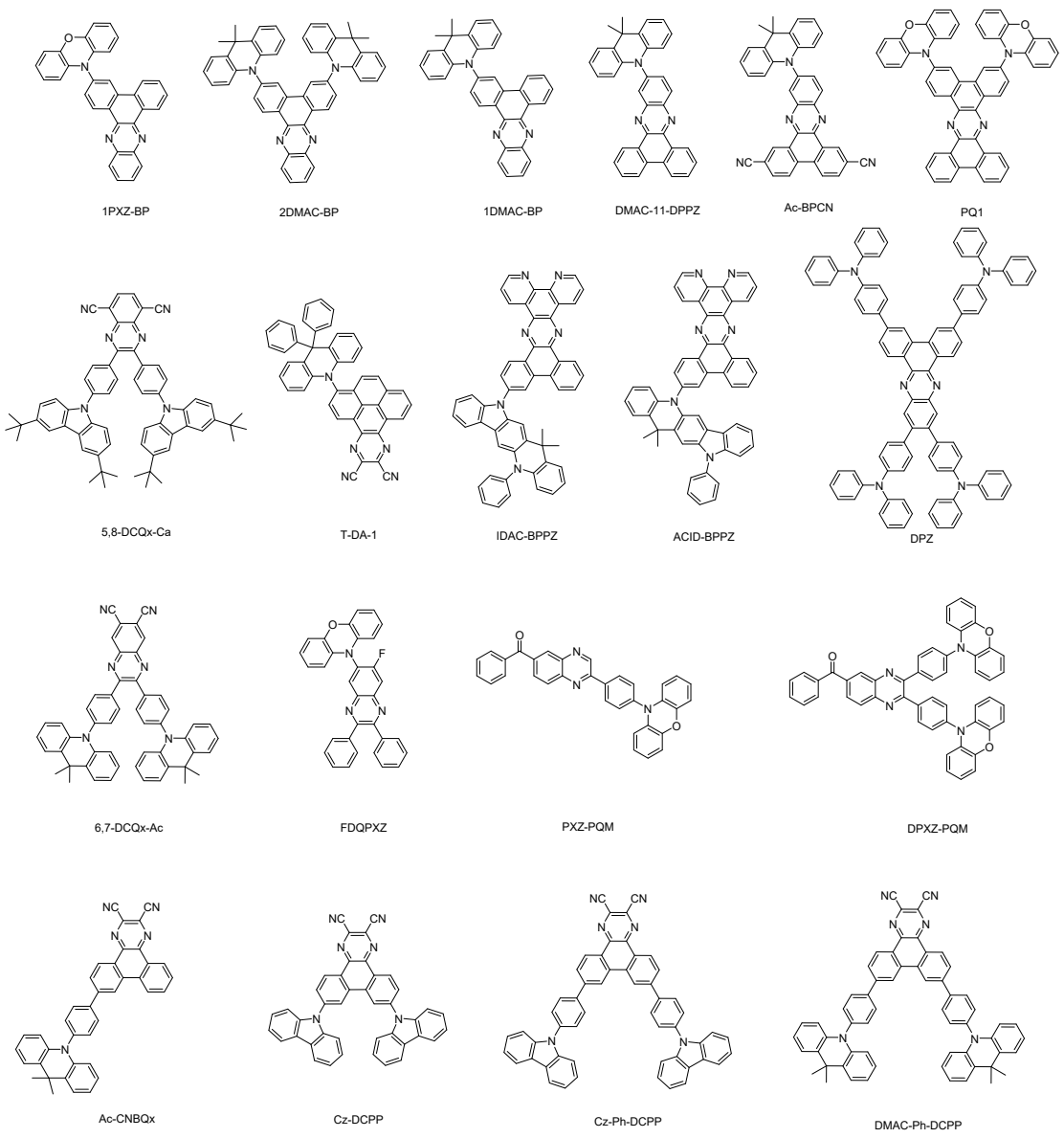

Figure S24. Chemical structures of emitters listed in Figure S23.

III. References

1. M. J. Frisch, G. W. Trucks, H. B. Schlegel, G. E. Scuseria, M. A. Robb, J. R. Cheeseman, G. Scalmani, V. Barone, B. Mennucci, G. A. Petersson, H. Nakatsuji, M. Caricato, X. Li, H. P. Hratchian, A. F. Izmaylov, J. Bloino, G. Zheng, J. L. Sonnenberg, M. Hada, M. Ehara, K. Toyota, R. Fukuda, J. Hasegawa, M. Ishida, T. Nakajima, Y. Honda, O. Kitao, H. Nakai, T. Vreven, J. A. Montgomery, Jr., J. E. Peralta, F. Ogliaro, M. Bearpark, J. J. Heyd, E. Brothers, K. N. Kudin, V. N. Staroverov, T. Keith, R. Kobayashi, J. Normand, K. Raghavachari, A. Rendell, J. C. Burant, S. S. Iyengar, J. Tomasi, M. Cossi, N. Rega, J. M. Millam, M. Klene, J. E. Knox, J. B. Cross, V. Bakken, C. Adamo, J. Jaramillo, R. Gomperts, R. E. Stratmann, O. Yazyev, A. J. Austin, R. Cammi, C. Pomelli, J. W. Ochterski, R. L. Martin, K. Morokuma, V. G. Zakrzewski, G. A. Voth, P. Salvador, J. J. Dannenberg, S. Dapprich, A. D. Daniels, O. Farkas, J. B. Foresman, J. V. Ortiz, J.

Cioslowski and D. J. Fox, Gaussian, Inc., Wallingford CT, 2013, Gaussian 09, Revision E.01.
2. X. Gao, S. Bai, D. Fazzi, T. Niehaus, M. Barbatti, W. Thiel, *J. Chem. Theory Comput*., 2017, **13**, 515-524.
3. T. Lu and F. Chen, *J. Comput. Chem.*, 2012, **33**, 580-592.
4. W. Humphrey, A. Dalke and K. Schulten, *J. Mole. Graph*., 1996, **14**, 33-38.
5. Y. Liu, J. Yang, Z. Mao, X. Chen, Z. Yang, X. Ge, X. Peng, J. Zhao, S. J. Su and Z. Chi, *ACS Appl. Mater. Interfaces,* 2022, **14**, 33606−33613.
6. F. M. Xie, P. Wu, S. J. Zou, Y. Q. Li, T. Cheng, M. Xie, J. X. Tang, X. Zhao, *Adv. Electron. Mater.* 2020, **6**, 1900843.
7. F. M. Xie, H. Z. Li, G. L. Dai, Y. Q. Li, T. Cheng, M. Xie, J. X. Tang, X. Zhao, *ACS Appl. Mater. Interfaces.* 2019, **11**, 26144-26151.
8. S. Kothavale, K. H. Lee, J. Y. Lee, *ACS Appl. Mater. Interfaces.* 2019, **11**, 17583-17591.
9. S. Kothavale, W. J. Chung, J. Y. Lee, *J. Mater. Chem. C.* 2020, **8**, 7059-7066.
10. U. Balijapalli, Y. T. Lee, B. S. B. Karunathilaka, G. Tumen-Ulzii, M. Auffray, Y. Tsuchiya, H. Nakanotani, C. Adachi, *Angew. Chem. Int. Ed.* 2021, **23**, 19364-19373.
11. S. Kothavale, K. H. Lee, J. Y. Lee, *ACS Appl. Mater. Interfaces.* 2019, **11**, 17583-17591.
12. T. Yang, Z. Cheng, Z. Li, J. Liang, Y. Xu, C. Li, Y. Wang, *Adv. Funct. Mater.* 2020, **30**, 2002681.
13. J.-X. Chen, W.-W. Tao, Y.-F. Xiao, S. Tian, W.-C. Chen, K. Wang, J. Yu, F.-X. Geng, X.-H. Zhang, C.-S. Lee, *J. Mater. Chem. C.* 2019, **7**, 2898-2904.
14. Y. Liu, J. Yang, Z. Mao, D. Ma, Y. Wang, J. Zhao, S. J. Su and Z. Chi, *Adv. Opt. Mater.*, 2022, 2201695.
15. L. Yu, Z. Wu, G. Xie, C. Zhong, Z. Zhu, H. Cong, D. Ma, C. Yang, *Chem. Commun.* 2016, **52**, 11012-11015.
16. J. Liang, C. Li, Y. Cui, Z. Li, J. Wang, Y. Wang, *J. Mater. Chem. C.* 2020, **8**, 1614-1622.
17. R. Furue, K. Matsuo, Y. Ashikari, H. Ooka, N. Amanokura, T. Yasuda, *Adv. Opt. Mater.* 2018, **6**, 1701147.
18. S. Wang, Z. Cheng, X. Song, X. Yan, K. Ye, Y. Liu, G. Yang, Y. Wang, *ACS Appl. Mater. Interfaces.* 2017, **9**, 9892-9901.